RSC Advances

PAPER

View Article Online
View Journal | View Issue

Cite this: *RSC Adv.*, 2020, **10**, 31979

In vitro anticancer activity of parent and nano-encapsulated samarium(III) complex towards antimicrobial activity studies and FS-DNA/BSA binding affinity

Saeid Asadpour, *[ab] Zahra Aramesh-Boroujeni *[cd] and Shohreh Jahani [e]

Received 16th June 2020
Accepted 11th August 2020

DOI: 10.1039/d0ra05280a

rsc.li/rsc-advances

Based on the potential anticancer properties of lanthanide complexes, the anticancer activity of the Sm(III) complex containing a 2,2′-bipyridine ligand (bpy) and its interaction with FS-DNA (Fish-Salmon DNA) and BSA (Bovine Serum Albumin) were examined experimentally and by molecular docking in this paper. Absorption and fluorescence spectroscopic methods were used to define the thermodynamic parameters, binding constant (K_b), and the probable binding mechanism. It was concluded that the Sm complex interacts with FS-DNA through a minor groove with a K_b of 10^5 M^{-1}. Also, the K_b for the BSA binding at 298 K was found to be 5.89×10^5 M^{-1}, showing relatively a high tendency of the Sm complex to DNA and BSA. Besides, the Sm complex was docked to BSA and DNA by the autodock program. The results of the docking calculations were in good agreement with the experimental examinations. Additionally, the antifungal and antibacterial properties of this complex were investigated. The anticancer tests on the effect of the Sm complex, starch nano-encapsulation, and lipid nano-encapsulation in MCF-7 and A-549 cell lines were performed by the MTT method. It can be observed that the Sm complex and its nanocarriers presented a selective inhibitory effect on various cancer cell growths.

1. Introduction

Lanthanide coordination chemistry has developed to cater to a varied range of applications. These compounds are used in luminescent biology sensors, materials science, and self-assemblies of contrast-enhancing factors, as well as in medicine such as anticancer, antibacterial, and fungicidal properties.[1–7] The binding of lanthanide compounds with macromolecules (*e.g.*, DNA and proteins) is an exciting part for both biochemists and inorganic chemists.[8,9]

The interactions of compounds with DNA propose that these compounds can have potential pharmaceutical and biological activities that depend on the affinity of the interaction mode with DNA. When designing potential antitumor factors, non-intercalation compounds are more favorable than intercalation compounds. Hence, abundant compounds produce considerable active antitumor factors that bind through grooves of DNA. Given the success in the tumor therapy of DNA groove binders, it is considered valuable to investigate the existing compounds as groove binders.[8] Furthermore, serum albumins are the most abundant protein in blood that show significant role in the distribution, metabolism, and transport of various exogenous compounds (containing drugs, amino acids, fatty acids, and pharmaceuticals).[10]

In continuation of recent research work,[11–17] the synthesis, characterization, and interaction of the Sm-complex, $[Sm(bpy)_2Cl_3(OH_2)]$ (Scheme 1), with FS-DNA and BSA by different types of experimental techniques and docking calculation are reported in this paper. Moreover, the parent, lipid nano-encapsulated (LNEP) and starch nano-encapsulated

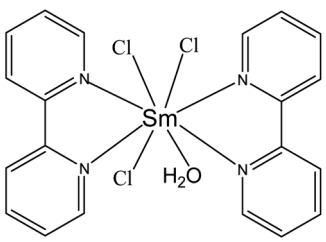

Scheme 1 Chemical structure of the Sm-complex.

[a]*Department of Chemistry, Faculty of Sciences, Shahrekord University, Shahrekord 115, Iran. E-mail: s.asadpour@sku.ac.ir*

[b]*Nanotechnology Research Center, Shahrekord University, 8818634141, Shahrekord, Iran*

[c]*Department of Clinical Laboratory, AlZahra Hospital, Isfahan University of Medical Sciences, Isfahan, Iran. E-mail: zaramesh.boroujeni@gmail.com*

[d]*Young Researchers and Elite Club, Najafabad Branch, Islamic Azad University, Najafabad, Isfahan, Iran*

[e]*Noncommunicable Diseases Research Center, Bam University of Medical Sciences, Bam, Iran*

(SNEP) forms of the Sm complex were prepared, and the anticancer properties of these compounds were assessed.

2. Experimental

2.1. Materials and instrumentation

FS-DNA was purchased from Fluka Biochemika, and other materials were obtained from Aldrich Chem. Co. and Merck. All solvents and chemicals were of analytical grade. The FT-IR spectra were performed as KBr pellets by a SHIMADZU spectrometer. The electronic spectra were carried out by a JASCO (V-670) spectrophotometer. Emission spectra were performed by PERKIN ELMER, LS-3. A model Perkin Elmer 240 elemental analyzer carried out the CHN (elemental) analyses, and a Bruker 400 Ultrashield NMR recorded the NMR spectra in D_2O. For determining the percentage of the Sm complex in LNEP and SNEP, these compounds were analyzed by an ICP-Spectro ciros CCD instrument (inductively coupled plasma spectrometer). The surface morphology of the LNEP and SNEP nanocomposites was examined with SEM, KYKY, EM 3200.

2.2. Synthesis and characterization of the samarium complex

The Sm complex was synthesized in accordance with the literature method.[18] An ethanolic solution (5 mL) of samarium chloride (100 mg, 2.74×10^{-4} mol) was added dropwise to the 2,2′-bipyridine (85.6 mg, 5.48×10^{-4} mol) dissolved in ethanol (5 mL). The resultant mixture was refluxed at 60 °C for four hours. After filtering the resulting precipitate, it was washed with cold ethanol and dried (yield 76%). Anal. found (calc.) ($C_{20}H_{18}Cl_3N_4OSm$): C, 40.75 (40.90); H, 3.10 (3.07); N, 9.64 (9.54). FT-IR (cm^{-1}): 1596 (C=N), 1434–1476 (C=C), 735–766 (C–H). ^1H NMR (400 MHz, D_2O): δ (ppm) 4.73 (H_2O, broad) and 8.32, 7.68, 7.22 (H-bpy, broad). Electronic absorption (H_2O): 231, 280 nm.

2.3. FS-DNA and BSA binding

All binding studies of the Sm complex were performed in tris(hydroxymethyl)-aminomethane at pH 7.2 (Tris–HCl buffer having NaCl (50 mM) and Tris (5 mM) and adjusted with HCl in pH = 7.2). The DNA concentration was defined spectrophotometrically with $\varepsilon_{260} = 6600\ M^{-1}\ cm^{-1}$ (the molar extinction coefficient at 260 nm). The absorbance ratio (A_{260}/A_{280}) was monitored to check the DNA purity. The absorbance proportion at 260 nm and 280 nm was in the range $1.8 < A_{260}/A_{280} < 2$ and showed that the DNA was free of protein and impurities.[19]

Moreover, the concentrations of EtBr and BSA were found by UV-vis spectrometry by assuming $\varepsilon_{480} = 5450\ M^{-1}\ cm^{-1}$ and $\varepsilon_{280} = 44\ 300\ M^{-1}\ cm^{-1}$ for EtBr and BSA, respectively.[20,21] All solutions were not used for more than four days, and also stored at four degrees Celsius. The stability of the Sm complex in aqueous solution was tested by monitoring the absorption spectrum of the Sm complex at different incubation times. The slight changes of the spectra after 48 hours showed the stability of the Sm complex during the interaction studies.

2.4. Docking setup

The Auto Dock 4.2.6 program was applied to perform the docking calculations by the Lamarckian genetic algorithm. The BSA structure (code: 3v03) and DNA sequence duplex (code: 1BNA) were obtained from the Protein Data Bank. The quantum chemical software was employed to optimize the Sm complex structure by DFT.[21,22] During the docking process, all complex bonds were kept free, while BSA and DNA stayed rigid. The grid map of $70 \times 70 \times 70$ points and 0.375 Å spacing were made. Next, 200 independent calculations with 25 million energy evaluations were obtained.[23]

2.5. Cytotoxicity

The LNEP and SNEP of the Sm complex were synthesized in accordance with the literature.[24] The anticancer properties of the terbium complexes, LNEP and SNEP, were studied by MTT examination on the A-549 and MCF-7 cell lines, as explained previously.[9] The unwanted cytotoxicity potential of these compounds was also studied on normal human fibroblast (HFB) cells. These cell lines were incubated for one day in a humidified 5% CO_2 incubator at 37 °C, in the presence of different concentrations of the Sm complex, SNEP, and LNEP. After this step, the solution of MTT (10 μL, 12 mM) was added, and then the plates were incubated for four hours. The culture media was rejected. After the addition of DMSO (50 μL), the wells were washed with phosphate-buffered saline and incubated for ten minutes. IC_{50} is the 50% inhibition concentration, which is calculated by an ELISA reader at 545 nm through the following eqn (1):[25]

$$\%\ \text{Cell cytotoxicity} = [1 - (\text{drug absorption}/\text{control absorption})] \times 100 \quad (1)$$

For evaluating the influence of SNEP and LNEP on the anticancer properties, the cellular penetration examination was performed. The cell lines of A-549, MCF-7 and HFB with the cell culture (100 μL) medium including 7.51 μg Sm complex (128 μM), 12.26 μg SNEP or 11.51 μg LNEP (equivalent to 7.51 μg Sm complex) were incubated for one day in a 5% CO_2 incubator. After eliminating the supernatant, these mixes (the cells having Sm-complex) were treated with $CHCl_3$ and HNO_3. All studies were done three times. Two commercial anti-cancer drugs of 5-fluorouracil (5-FU) and methotrexate were used as a positive control under the same conditions.[26]

2.6. Microbiological investigations

The zone of inhibition testing, the plate-counting technique, the minimum inhibitory concentration (MIC), and the inoculation time were applied to determine the antimicrobial activity of the Sm-complex against MRSA, VRE, *E. faecium*, *E. faecalis*, *P. aeruginosa*, *A. baumannii*, *E. coli*, *K. pneumonia*, *S. typhi*, and fungi *C. albicans*.[27,28] In addition, chloramphenicol was used as a positive control.

In the inhibition zone diameter method, a stock inoculum with 700 CFU mL^{-1} was applied for dyes on the Muller Hinton (MH) agar plate. Afterward, discs of filter paper saturated with

the antimicrobial matter (Sm-complex, 5 mg mL^{-1}) were transported on the agar. The incubation was carried out at 37 °C for one day to take the zone of inhibition. The broth dilution technique was used for the plate-counting methods and MIC. Tubes containing MH broth (5.0 mL) with ten-fold dilutions of antimicrobial agents (0.005–50 mg L^{-1}) were inoculated with 700 CFU mL^{-1} of bacteria and fungi. The tubes were also incubated at 37 degrees centigrade for one day. Then, the incubation tubes were studied without shaking for visible turbidity. The MIC was found as the lowest dilution of this compound that produced no noticeable turbidity.

After the minimum inhibitory concentration was detected, 0.1 mL of inoculum from the content of the tube, without visible turbidity was subculture onto the agar plate and also incubated for one day. Then, the number of grown colonies on the subculture was contrasted to the number of CFU mL^{-1} in the initial inoculum. The minimum bactericidal concentration (MBC) was referred to as the lowest dilution of the lanthanide compound, which allowed for less than 0.1% of the initial inoculum to live. These studies were performed three times.

3. Results and discussion

3.1. Spectral characterization

In Fig. 1(A), the infrared spectrum of the free ligand was compared with that of the Sm complex to define the deviances that may have to happen with complexation. The infrared spectrum of 2,2′-bipyridine indicated the peaks in the frequency range of 1596, 1434–1476, and 735–766 cm^{-1} for ν(C=N), ν(C=C) and ν(C–H), respectively. In the Sm complex, these bands shift significantly to a lower wavenumber. Moreover, the IR spectrum of the Sm complex indicated new peaks at 423 and 3000–3356 cm^{-1} ascribable to the Sm–N and O–H stretching vibrations, respectively.[29]

Fig. 1(B) displays the UV-vis spectra of the Sm complex in various solvents, where the changes of the maximum absorption wavelength (λ_{max}) were apparent. The polarity of the solvent was the chief cause, which affects λ_{max}. Depending on the solute–solvent bindings, the energy of the excited and ground states of the solute may decrease or increase. Therefore, λ_{max} changes to higher or lower values. The UV-vis spectra of the Sm complex indicated two peaks in the range of 215–320 nm. From Fig. 1(B), by replacing the solvent from water to acetonitrile, a redshift of the n→π* transition band (λ_{max} values were 280, 284, and 281 nm in water, acetonitrile, and methanol, respectively) was detected. The ^{1}H NMR spectrum of the Sm-complex displayed three broad bands at 7.22, 7.68, and 8.32 ppm, which were equivalent to the aromatic ring protons, and a broad band at 4.73 ppm equivalent to the hydrogen of water. In the Sm complex, the ^{1}H NMR spectra underwent massive changes and shifts in comparison with the free ligand spectra.[30] This shows a reduction in the deshielding effect of the electron density in the aromatic ring after coordination to the Sm ion.

3.2. DNA binding experiments

3.2.1. UV-vis spectroscopy. Generally, when a compound interacts with DNA, changes in the UV-vis spectra should occur.[31] A hyperchromic result without a redshift proposes the occurrence of groove binding or an electrostatic interaction between DNA and the complexes. A hypochromic result, along with a redshift of the absorption spectrum (bathochromic effect), remains as the typical characteristic of the intercalation mode.[32] The electronic spectra of the samarium complex with increasing DNA concentration are presented in Fig. 2(A). With increasing FS-DNA concentration, a reduction in the intensity of the complex absorption peak without a shift in the absorption peak was detected, which illustrates the existence of the groove binding between FS-DNA and the Sm-complex. The intrinsic binding constant (K_b) was calculated by eqn (2):[31]

$$[Q]/(\varepsilon_a - \varepsilon_f) = [Q]/(\varepsilon_b - \varepsilon_f) + 1/K_b(\varepsilon_b - \varepsilon_f) \quad (2)$$

In the above equation, the extinction coefficients ε_f, ε_b, and ε_a correspond to the extinction coefficients for the Sm-complex in a free state, the fully bound form, and A_{obsd}/[Complex], respectively, and [Q] is the FS-DNA concentration. K_b at 298 K was 1.20×10^5 M^{-1} (Fig. 2(B)), which was lower than that of the classic intercalation compound, EtBr (1.4×10^6 M^{-1}).[33] The binding mode between the Sm-complex and FS-DNA (non-intercalation) was revealed to be different from that of EtBr (intercalation).

3.2.2. Emission experiments. The emission experiment is an effective method for evaluating the interaction mode of compounds to macromolecules, such as DNA and proteins. Fixed amounts (1×10^{-7} M) of the Sm(III) complex were titrated with enhancing FS-DNA concentration. This Sm-complex emits fluorescence in the range of 300–500 nm from excitation at λ_{ex} = 280 nm. The Sm complex

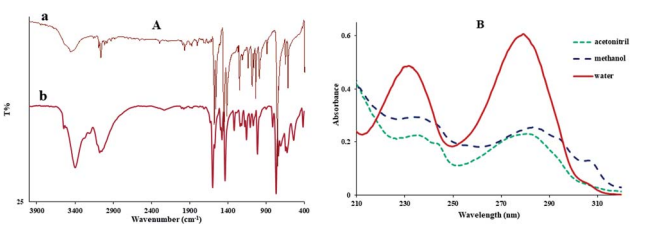

Fig. 1 (A) FT-IR spectra of (a) 2,2′-bipyridine ligand, (b) Sm complex. (B) The UV-vis spectra of the Sm-complex in different solvents ([Sm-complex] = 1×10^{-5} M).

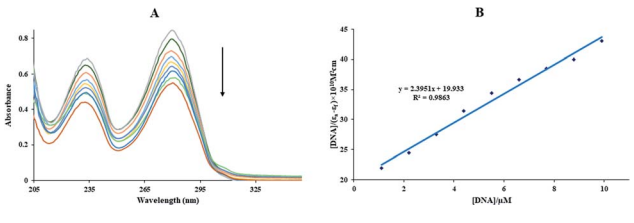

Fig. 2 (A) Electronic spectra of Sm(III) complex in the presence and absence of different concentrations of DNA, [DNA] = 1.1–9.9 μM and [Complex] = 1×10^{-5} M. T = 298 K. (B) The plot of [DNA]/($\varepsilon_a - \varepsilon_f$) *versus* [DNA].

emission spectra in the presence of DNA at 25 °C are revealed in Fig. 3(A). As seen with increasing FS-DNA amounts, the intensity of the Sm-complex emission was reduced. The quenching occurrence of the Sm complex emission by FS-DNA can be ascribed to the photoelectron transfer from the guanine base of DNA to the Sm-complex, exciting states.[34]

Quenching can occur by various mechanisms, which are generally categorized as dynamic (the collisional procedure) and static quenching (the formation of the fluorophore–quencher system in the ground state). Generally, the static and dynamic quenching mechanisms were determined by the excited-state lifetime and study of the temperature on the Stern–Volmer equation (eqn (3)).[34,35] eqn (3) explains the emission quenching process:

$$\frac{F_0}{F} = 1 + K_{SV}[Q] = 1 + K_q\tau[Q] \quad (3)$$

In the above equation, K_{SV} is the quenching constant, [Q] is the FS-DNA concentration, F_0 and F express the emission intensity in the absence and presence of FS-DNA, respectively. This equation τ_0 is the fluorophore lifetime without any quencher ($\tau_0 = 10^8$ s) and k_q is the fluorophore quenching rate constant. The K_{SV} and k_q values were found at various temperatures, and these values are presented in Table 1 and Fig. 3(B). In this study, the k_q amounts (in the area of 10^{12} M^{-1} s^{-1}) were higher than the maximum of k_q in the biomolecules (2.0×10^{10} M^{-1} s^{-1} (ref. 36)), indicating that the emission quenching generally occurred from static quenching instead of collision quenching. From Table 1, with the temperature increasing from 296 K to 303 K, K_{SV} slightly increased from 6.66×10^5 M^{-1} to 8.17×10^5 M^{-1}, while the high value of K_{SV} was due to the collision quenching. Thus, we proposed that the probable quenching mechanism may be static. The binding stoichiometry (n) and K_b for the binding between FS-DNA and the Sm complex were determined using the following equation:

$$\log\frac{F_0 - F}{F} = \log K_b + n\log[Q] \quad (4)$$

The K_b values of the Sm-complex were found at 296, 298, 301, and 303 K (Table 1 and Fig. 3(C)). Since the n values were close to 1, this showed that there was just one binding site. The K_b values confirmed the considerable high affinity of FS-DNA to the Sm-complex.

According to the values of the entropy change (ΔS°) and enthalpy change (ΔH°), the nature of the interaction between the complex and biomacromolecules (such as proteins and DNA) can be concluded as follows: (1) $\Delta S^\circ > 0$ and ΔH° close to 0, electrostatic interactions; (2) $\Delta S^\circ < 0$ and $\Delta H^\circ < 0$, hydrogen bond and van der Waals interactions; (3). $\Delta S^\circ > 0$ and $\Delta H^\circ > 0$, hydrophobic forces. For discriminating the binding model between FS-DNA and the Sm complex, ΔS°, ΔH° and the free energy change (ΔG°) can be given by the following eqn (5) and (6):

$$\ln K_b = -\frac{\Delta G^\circ}{RT} = -\frac{\Delta H^\circ}{R}\left(\frac{1}{T}\right) + \frac{\Delta S^\circ}{R} \quad (5)$$

$$\Delta G^\circ = \Delta H^\circ - T\Delta S^\circ \quad (6)$$

The linear van't Hoff plot based on ln K against $1/T$ (Fig. 3(D)) allows for acquiring ΔH°, ΔS°, and ΔG° (eqn (6)). Table 1 reveals the thermodynamic values of the Sm complex. The positive signs of ΔS° and ΔH° exposed that hydrophobic binding plays the main role in the interaction of FS-DNA with the Sm complex.

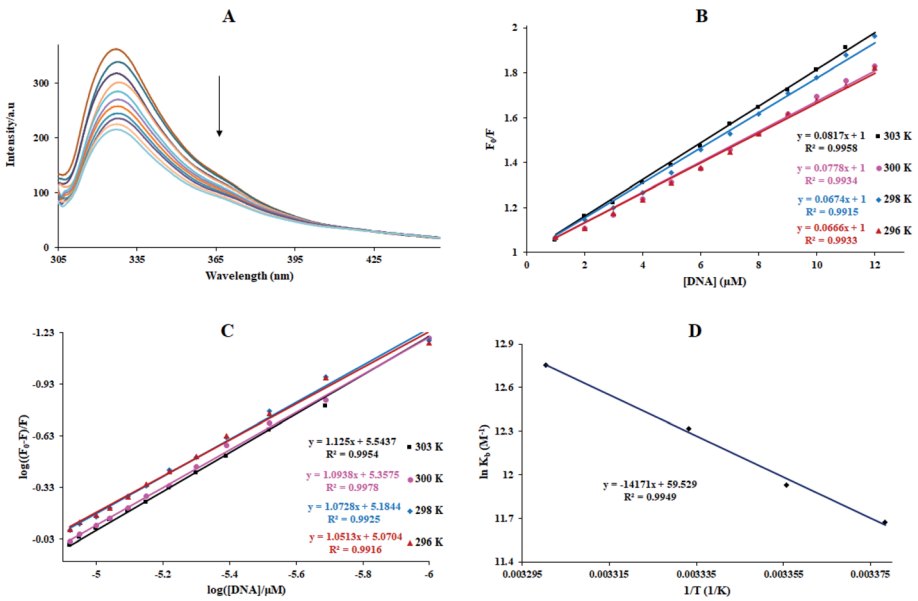

Fig. 3 (A) The fluorescence spectra of the Sm(III) complex in the presence and absence of different concentrations of DNA, [DNA] = 0 to 14.3 μM and [Complex] = 1×10^{-7} M (λ_{ex} = 280 nm, pH = 7.2 and T = 298 K). (B) Stern–Volmer curves, (C) Plots of log(($F_0 - F$)/F) against log([DNA]/μM) for the complex at 296, 298, 300 and 303 K, (D) van't Hoff plot for the interaction of DNA with the Sm(III) complex.

Table 1 The binding constant (K_b), the number of binding sites (n), the biomolecular quenching rate constant k_q, the Stern–Volmer constant (K_{SV}), and thermodynamic parameters (ΔS°, ΔH°, and ΔG°) for the interaction of DNA with the Sm-complex at various temperatures

				$K_b \times 10^{-5}$ (M^{-1})				
T (K)	$K_{SV} \times 10^{-4}$ (M^{-1})	$k_q \times 10^{-12}$ (M^{-1} s^{-1})	n	UV	Fluorescence	ΔG° (kJ mol^{-1})	ΔH° (kJ mol^{-1})	ΔS° (J mol^{-1} K^{-1})
296	6.66 ± 0.04	6.66 ± 0.04	1.05		1.17 ± 0.03	−28.73 ± 0.02		
298	6.74 ± 0.05	6.74 ± 0.05	1.07	1.20 ± 0.04	1.51 ± 0.05	−29.55 ± 0.05	117.82 ± 0.05	494.92 ± 0.03
300	7.78 ± 0.03	7.78 ± 0.03	1.09		2.24 ± 0.02	−30.72 ± 0.03		
303	8.17 ± 0.02	8.17 ± 0.02	1.12		3.47 ± 0.05	−32.13 ± 0.04		

Also, the negative value of ΔG° showed that the DNA binding process was spontaneous.

3.2.3. KI quenching experiment. The emission quenching of the Sm-complex was examined by potassium iodide as the ionic quencher. The intercalative interaction of the DNA base-pairs with the compounds protected the compounds from ionic quenchers. Hence, they displayed very little quenching compared with the aqueous solution. In contrast, in the groove binding interaction, the compounds were subjected to the aqueous solution. This made the compound quite available to the quenchers.[37] The emission spectroscopy of the Sm complex was compared with that of the Sm complex-DNA mixture during the regular addition of I^-. As seen in Fig. 4, I^- quenched the Sm complex emission in the presence ($K_{SV} = 26.37\ M^{-1}$) and absence of FS-DNA ($30.34\ M^{-1}$). These data propose that FS-DNA interacts with the Sm complex through the groove binding interaction.

3.2.4. Competitive displacement assays. As we know, the interaction type of EtBr on DNA is intercalation. EtBr was commonly used as a sensitive probe to study the pattern of interaction of DNA to compounds.[37] EtBr emits an intense fluorescence in the presence of DNA because it can intercalate the double-helical DNA. The intercalative complexes will replace ethidium bromide in the DNA complex, causing a considerable decrease in fluorescence intensity of the EtBr–DNA complex.[37–39] The fluorescence spectra of EtBr bound to FS-DNA in the presence and absence of the Sm(III) complex are revealed in Fig. 5(A). When excited at 525 nm, the DNA–EtBr complex illustrates a maximum emission at 586 nm. When the Sm-complex was added to the EtBr–DNA complex, an insignificant decrease in the fluorescence intensity was detected. It stopped reducing the intensity at about 9.3% of the initial intensity (Fig. 5(B)). This result suggested that the Sm-complex did not exchange EtBr molecules, and the interaction of the DNA with the Sm complex was not equal to that of ethidium bromide.

3.2.5. Salt concentration effect. Observing the spectral change with different ionic strengths is an important way to discriminate the nature of the DNA interaction with the compounds. The addition of the sodium cation weakened the electrostatic binding of DNA to the compounds because of the competition from the phosphate backbones.[37,40] The influence of sodium chloride on the emission of the Sm complex in the presence and absence of FS-DNA (4.4 μM) was examined. The results showed that with increasing NaCl concentration (0.05 to 0.6 M), the fluorescence intensity of the Sm complex did not considerably change. This proposed a non-electrostatic interaction of DNA with the Sm complex.

3.2.6. Viscosity study. The viscosity experiments found further evidence of the interaction mode of FS-DNA with the Sm complex. The classical intercalation was estimated to lengthen the DNA due to the base pair separation at the site of intercalation, leading to a concomitant enhancement in the DNA viscosity. On the contrary, partially interacting compounds and the groove binders caused no effect or had only a slight effect on the DNA solution viscosity.[37,41] The relative specific viscosity values $(\eta/\eta_0)^{1/3}$ against ([Complex]/[DNA]) were planned, where η and η_0 correspond to the accurate DNA viscosity contributions in the presence and absence of the Sm complex, respectively. It can be seen that with increasing complex amount, an insignificant change in the FS-DNA viscosity was observed. It was evidenced from the other techniques that the binding between FS-DNA and the Sm complex belonged to the groove-binding mode.

3.3. Protein-binding

3.3.1. Electronic spectroscopy. Absorption spectroscopy is an important technique to detect the structural changes of

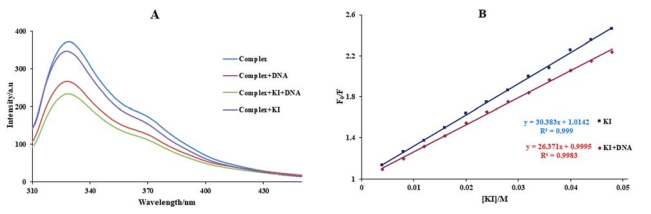

Fig. 4 (A) The emission spectra of KI quenching for the DNA-complex system, [DNA] = 4.4 μM, [KI]: 4.0–40.0 mM and [Complex]: 0.1 μM. (B) Stern–Volmer plot of the emission titration data of the Sm-complex.

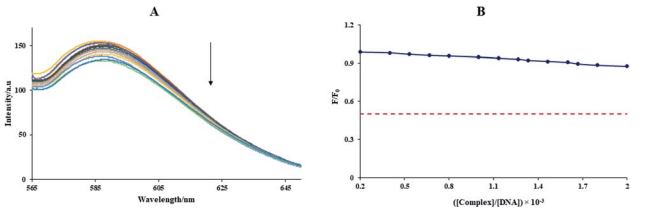

Fig. 5 (A) The emission quenching curves of EtBr bound to DNA by the Sm(III) complex ([EtBr] = 8.3 μM, [DNA] = 140 μM, [Complex] = 0–145.7 μM). (B) The plot of F/F_0 against ([Complex]/[DNA]).

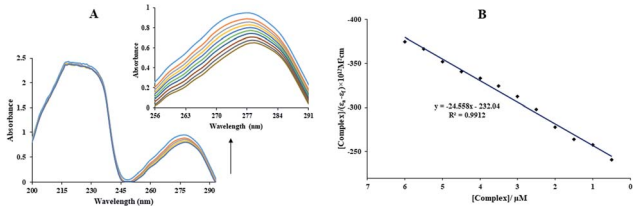

Fig. 6 (A) UV-vis spectra of BSA in the presence and absence of different concentrations of the Sm(III) complex, [BSA] = 10 μM, [Complex] = 0.5–6.0 μM. (B) The plot of [Complex]/($\varepsilon_a - \varepsilon_f$) *vs.* [Complex].

proteins. The BSA solution indicated two absorption bands: a sharp band at 215 nm and a weak band at 280 nm. This could be reflected in the BSA framework conformation and was determined by the polarity of the environment around the Trp, Tyr, and Phe residues.[20,42] Fig. 6(A) illustrated the BSA absorption spectra (10 μM) with the addition of enhancing the concentration of the Sm complex (0.5–6.5 μM). Fig. 6(A) shows that upon increasing the complex concentrations to BSA, the band intensity is enhanced without any considerable change in the peak situation (Fig. 6(A)). These results confirm that the BSA bends with the Sm(III) complex, and also does not change the polarity of the environment around the amino acid residues. The K_b can be given from eqn (2) (Fig. 6(B)).

The K_b at 298 K was found to be 1.06×10^5 M^{-1} for the BSA–Sm complex. It is well-known that K_b in the range of 10^4 to 10^6 M^{-1} is acceptable for the carrier-drug compounds.[20] Thus, the K_b value of the Sm complex shows that this protein can be considered a suitable carrier for the Sm complex transfer in blood.

3.3.2. Emission studies. The emission spectra were applied to estimate the binding of BSA with compounds because the intrinsic emission of BSA is very sensitive to the microenvironment change. The BSA emission spectra (3.0 μM) with the different Sm complex amounts (0.5 to 6.0 μM) are revealed in Fig. 7(A). With increasing complex concentration, a regular reduction in the fluorescence intensity was detected. The

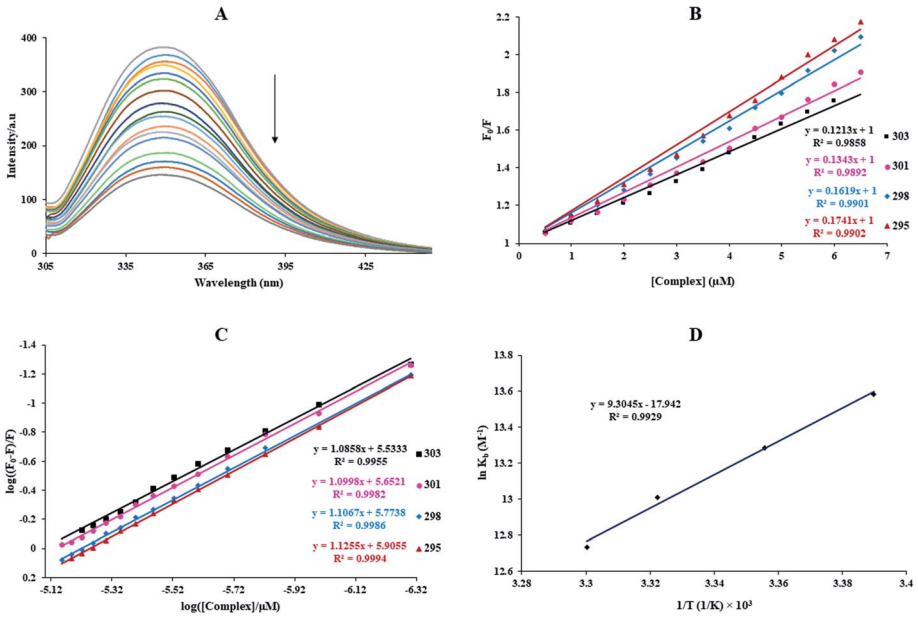

Fig. 7 (A) The BSA fluorescence spectra in the absence and presence of different concentrations of the Sm(III) complex, [BSA] = 3 μM and [Complex] = 0.5 to 6.0 μM (T = 298 K and λ_{ex} = 280 nm, pH = 7.2). (B) Stern–Volmer curves, (C) Plots of log(($F_0 - F$)/F) *versus* log([Complex]/μM) for the binding of the complex with BSA at 295, 298, 301 and 303 K. (D) van't Hoff plot for the binding of the Sm(III) complex with BSA.

Table 2 The binding constant (K_b), the number of binding sites (n), the biomolecular quenching rate constant k_q, the Stern–Volmer constant (K_{SV}), and thermodynamic parameters (ΔS°, ΔH°, and ΔG°) for the interaction of BSA with the Sm-complex at various temperatures

				$K_b \times 10^{-5}$ (M^{-1})				
T (K)	$K_{SV} \times 10^{-5}$ (M^{-1})	$k_q \times 10^{-12}$ (M^{-1} s^{-1})	n	UV	Fluorescence	ΔG° (kJ mol^{-1})	ΔH° (kJ mol^{-1})	ΔS° (J mol^{-1} K^{-1})
295	1.74 ± 0.05	1.74 ± 0.05	1.12		7.94 ± 0.04	−33.32 ± 0.03		
298	1.62 ± 0.04	1.62 ± 0.04	1.10	1.06 ± 0.03	5.89 ± 0.04	−32.92 ± 0.04	−77.35 ± 0.03	−149.17 ± 0.04
301	1.34 ± 0.04	1.34 ± 0.04	1.09		4.47 ± 0.05	−32.55 ± 0.04		
303	1.21 ± 0.03	1.21 ± 0.03	1.08		3.39 ± 0.02	−32.07 ± 0.05		

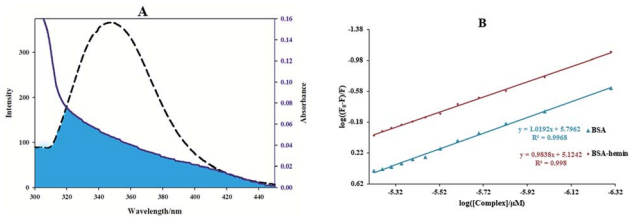

Fig. 8 (A) The overlap of the fluorescence spectrum of BSA (dashed lines) and the UV-vis spectrum (solid lines) of the Sm(III) complex. The molar ratio of BSA to Sm-complex was 1. (B) Effect of the site marker to the Sm–BSA system, Plots of $\log((F_0 - F)/F)$ against $\log([\text{Complex}]/\mu\text{M})$ ([Sm-complex] = 0.5–6.0 μM, [Hemin] = 0.3 μM, [BSA] = 3 μM, and λ_{ex} = 280 nm).

Table 3 The overlap integral (J), Förster critical distance (R_0), the binding distance to the protein tryptophan residue (r), and the energy transfer efficiency (E) in the binding of BSA with the Sm-complex ([Sm complex] = [BSA] = 3 μM, and λ_{ex} = 280 nm)

E	J (cm^3 L mol^{-1}) × 10^{-13}	R_0 (nm)	r (nm)
0.22	4.65	2.23	2.77

quenching of the BSA fluorescence showed that an interaction of BSA with the Sm complex indeed existed.

For studying the quenching process, the emission quenching data of k_q and K_{SV} are given by the eqn (3), and also revealed in Table 2 and Fig. 7(B). As shown in Fig. 7 and Table 2, K_{SV} was reduced and the k_q values were more significant than 2.0×10^{10} M^{-1} s^{-1} (the maximum k_q of the biomolecules) with increased temperature. It is plausible that the possible quenching mechanism of the interaction of BSA to the Sm complex was static.

The numbers of binding sites and the K_b at different temperatures for the binding of BSA with the complex can be calculated by eqn (4), and is indicated in Table 2 and Fig. 7(C). The K_b value for the Sm complex was determined to be 5.89 ± 0.04 × 10^5 M^{-1} at room temperature. The n in BSA was approximated to 1, showing that a single site in BSA was reactive to the Sm-complex. The result showed that there was a strong interaction force of BSA with the Sm complex.

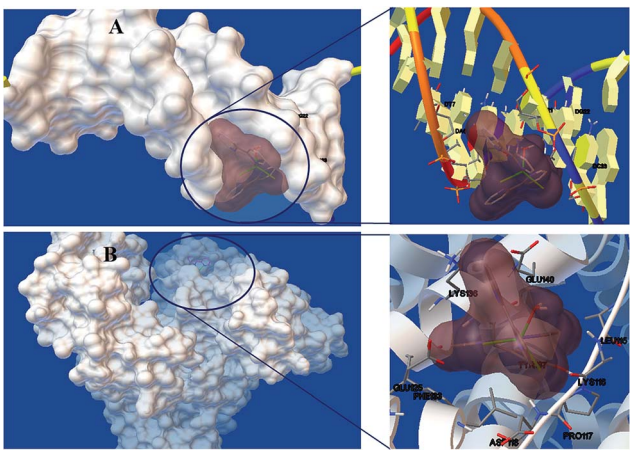

Fig. 9 Detailed view of the interactions between the Sm-complex and (A) DNA and (B) BSA.

Table 4 The inhibition constants and the binding energies of the Sm-complex for DNA and the BSA binding site

Macromolecule	Binding energy (kcal mol^{-1})	K_i (μM)
DNA	−7.51	3.25
BSA	−6.95	8.69

The van't Hoff equation was performed to give the thermodynamics parameters (ΔS°, ΔH°, and ΔG°) of the Sm complex–BSA system. The obtained thermodynamic parameters for the interaction of BSA with the Sm complex are listed in Table 2. Both negative signs of ΔS° and ΔH° indicated that the BSA–complex interaction was an entropic and exothermic reducing process, and the negative signs of ΔG° showed that the BSA binding procedure was spontaneous. In addition, hydrogen bonds and van der Waals forces play a significant role in this procedure.[43]

3.3.3. Binding distance and energy transfer. FRET (fluorescence resonance energy transfer) happens when the electronic spectrum of a compound (Sm complex, acceptor) overlaps with the emission spectrum of a fluorophore (protein, donor).[39] The shadowed section of Fig. 8(A) illustrates the spectral overlap between the electronic spectrum of the Sm complex and the BSA fluorescence spectrum. The noticeable overlap showed that there was a direct resonance energy transfer from protein to the Sm-complex. According to FRET theory, the distance (r) from Trp-214 of the protein to the complex and the energy transfer efficiency (E) were determined by eqn (7):

$$E = 1 - \frac{F}{F_0} = \frac{R_0^6}{R_0^6 + r^6} \quad (7)$$

where F and F_0 are the BSA emission intensities in the presence and absence of the Sm complex. R_0 is the critical distance when the transfer efficiency is 50%, and R_0 can be determined using eqn (8):

$$R_0^6 = 8.79 \times 10^{-25} K^2 n^{-4} \varnothing J \quad (8)$$

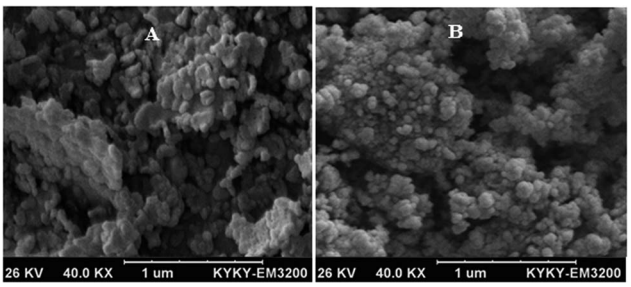

Fig. 10 SEM images of (A) SNEP and (B) LNEP.

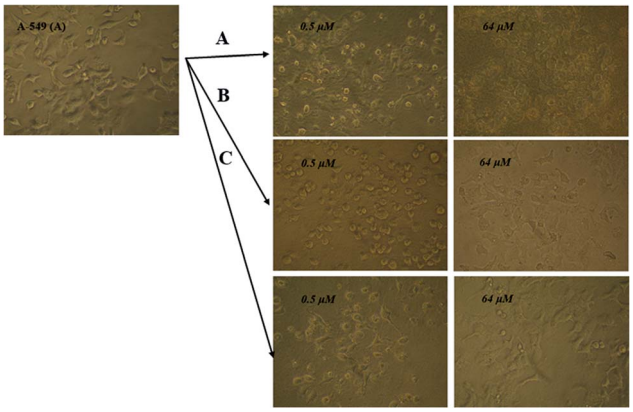

Fig. 11 Microscopic photographs of the A-549 cancer cells in the presence and absence of various concentrations of (A) LNEP, (B) SNEP and (C) Sm-complex.

where n is the medium refractive index, $\varnothing$ is the emission quantum yield of BSA, K^2 is the spatial orientation factor, and J is the overlap integral of the UV-vis and emission spectra. eqn (9) can give J:

$$J = \frac{\sum F(\lambda)\varepsilon(\lambda)\lambda^4\Delta\lambda}{\sum F(\lambda)\Delta\lambda} \quad (9)$$

Herein, $\varepsilon(\lambda)$ is the molar electronic coefficient of the Sm complex at wavelength λ, and $F(\lambda)$ is the BSA fluorescence intensity. In the study conditions, $K^2 = 2/3$, $n = 1.336$ and $\varnothing = 0.15$.[44] Accordingly, the R_0, r, J values, and E were determined and are listed in Table 3. All of the r and R values are $0.5R_0 < r < 1.5R_0$, and on the 2–8 nm scale, showing that the energy transfer between BSA and Sm-complex has occurred.[39]

3.3.4. Competitive studies for protein. The site marker competitive experiment was done to expose the Sm complex interaction site on the protein with site III marker (hemin), which specifically interacts with BSA.[45] With the addition of hemin to BSA, the emission intensity of the BSA solution was regularly reduced. It was much lower than that without hemin (site marker). It also showed that the bound BSA to the Sm complex was obtusely affected by the addition of hemin. The K_b value in the presence and absence of hemin (6.17×10^5 M^{-1} and 1.32×10^5 M^{-1}, respectively) was analyzed using eqn (4), and revealed that there was a significant competition between the hemin and Sm complex (Fig. 8(B)). Thus, the comparison of the K_b values showed that the Sm complex competed with hemin for the site III (subdomain IB) of BSA.

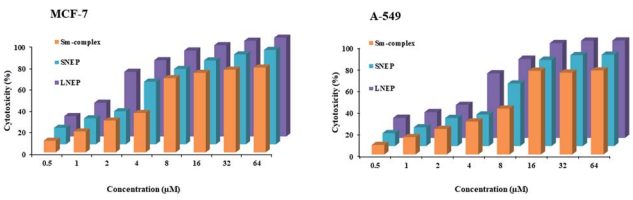

Fig. 12 Plots of cytotoxicity percentage various concentrations of the Sm-complex, SNPE and LNEP against the MCF-7 and A-549 cell lines.

Table 5 The IC_{50} of the Sm-complex, SNEP, LNEP, 5-fluorouracil, and methotrexate against the cell lines of A-549, MCF-7 and HFB

	The drug concentration causing a 50% reduction in cellular viability (IC_{50}) (μg mL^{-1})				
Cell lines	Sm-complex	SNEP	LNEP	5-fluorouracil	Methotrexate
MCF-7	5.78	3.42	1.65	47.5	27.9
A-549	9.5	6.91	3.35	43.9	26.9
HFB	105.4	103.2	104.6	50.8	36.0

3.4. Docking studies

3.4.1. Docking study with DNA. Molecular docking is extensively applied in the design of novel drugs. Today, this technique has provided an understanding of the mode and strength of the binding interactions between compounds and macromolecules.[37] The most energetically favorable structure of the docked position showed that the Sm complex approached the minor grooves of DNA. The lowest binding energy of DNA to the Sm complex was obtained at −7.51 kcal mol^{-1} (Fig. 9(A) and Table 4). The presence of a nonpolar fragment and polar groups (hydroxy) in the Sm complex assisted in the binding with DNA. Thus, considering the results of the theoretical calculations and the experimental methods, it could be concluded that the samarium complex interacted through groove binding.

3.4.2. Docking study with BSA. The specific binding of BSA with the Sm complex is illustrated in Fig. 9(B). According to the results from the docking calculations of the Sm complex with BSA, the binding energy of the docked structure is 6.95 kcal mol^{-1}. An analysis of the docking and conformation showed that the Sm complex interacted with the following residues: LEU115, LYS116, PRO117, ASP118, LEU122, GLU125, PHE133, LYS136, TYR137 and GLU140 (Fig. 9(B)). Some polar residues that interacted with the Sm complex cause the Sm complex to interact easily with BSA *via* non-covalent interactions, as well as groove binding (van der Waals). Also, docking studies of the other sites of BSA illustrated that the Sm complex has a greater binding affinity in site III (subdomain IB), where it approximately confirmed the competition studies.

3.5. Anticancer activity

3.5.1. Characterization of SNEP and LNEP. The SEM images of LNEP and SNEP are indicated in Fig. 10. It can be seen that the LNEP and SNEP average sizes were 50.4 and 48.5 nm, respectively. Also, the particle size of the Sm complex in LNEP was smaller than that in SNEP.

3.5.2. Anticancer assay. As the Sm(III) complex can actively interact with DNA, the anticancer activities of LNEP, SNEP, and the Sm complex against the cell lines of A-549 and MCF-7, as well as normal human fibroblast (HFB) were studied by the MTT method. Fig. 11 shows the microscopic analyses of the A-549 cells in the presence and absence of various amounts of the Sm(III) complex and its nanocarriers. Moreover, Fig. 12 shows

Table 6 The antibacterial and antifungal activities of the Sm-complex by the zone of inhibition (mm), minimum inhibitory concentrations (MIC, μg mL^{-1}), minimum bactericidal concentrations (MBC, mg mL^{-1}) and inoculation time (h) against fungi and bacteria

Bacteria type	Bacteria or fungi	Inoculation time (h)	Zone of inhibition (mm)	MIC (μg mL^{-1})	MBC (mg mL^{-1})
Fungi	*C. albicans*	24	40	31	1.0
Gram-negative	*E. coli*	48	12	62	4.0
	A. baumannii	48	25	31	2.0
	P. aeruginosa	48	21	62	4.0
	K. pneumoniae	24	18	125	1.0
	S. typhi	24	19	62	2.0
Gram-positive	VRE	24	28	125	4.0
	E. faecalis	48	26	31	4.0
	E. faecium	48	24	62	4.0
	MRSA	24	32	62	2.0

a plot of the cytotoxicity percentage against the Sm(III) complex concentration, SNEP, and LNEP. These results showed a reduction in the cancer cell number by enhancing these compound concentrations. The values of IC_{50} found for the complex, SNEP, and LNEP are listed in Table 5. The maximum cell inhibition was detected at a concentration of 64 μM. These data showed that the IC_{50} value found for this SNEP and LNEP was smaller than the IC_{50} value of the Sm complex. Thus, the diffusion of the Sm complex into tumor cells can be simplified by the lipid and starch, and its anti-cancer properties can be enhanced. As no significant difference was observed in the toxicity of the Sm-complex and its nano-carriers on the HFB cells (the IC_{50} values of the Sm-complex are 105.4 μg mL^{-1}).

The comparison of the anticancer activity and cytotoxicity effects of 5-fluorouracil and methotrexate as well-known commercial anticancer drugs, with the Sm-complex, SNEP, and LNEP (Table 5), emphasized the comparable anticancer activity and reduced toxicity of the Sm-complex and its nano-carriers.

3.6. Antimicrobial assay

Different methods were used to investigate the antimicrobial activity of the Sm-complex against bacteria and fungi. Table 6 reports the values of the zone of inhibition, inoculation time, MBC, and MIC. These complexes displayed significantly enhanced properties against different bacteria and fungi, especially *C. albicans*, *A. baumannii, E. coli*, and MRSA.

The MIC values for MRSA, *S. typhi*, *P. aeruginosa*, *E. coli* and *C. albicans* were found to be 62, 62, 62, 62 and 31 μg mL^{-1} for Sm-complex, respectively, which are very close to the positive control chloramphenicol. The MIC values for chloramphenicol are 62, 125, 31, 62 and >1000 μg mL^{-1}, respectively, for MRSA, *S. typhi*, *P. aeruginosa*, *E. coli* and *C. albicans*.

An effect of this lanthanide complex concentration with 700 CFU of *S. typhi* illustrations is shown in Fig. 13(A). The substantial decrease in the extent of bacterial colonies was detected in 4.0 mg of the Sm-complexes, displaying the antimicrobial properties upon increasing the Sm complex concentrations. The MH standard with 5 mg mL^{-1} of Sm-complex and 700 CFU of *S. typhi* supplemented for various time distances. Fig. 13(B) and Table 6 showed that the *S. typhi* colonies were killed entirely after 24 hours of injection of the Sm-complex, and the calculation of the bacterial reduction was nearly 100% after 4–48 hours of vaccination.

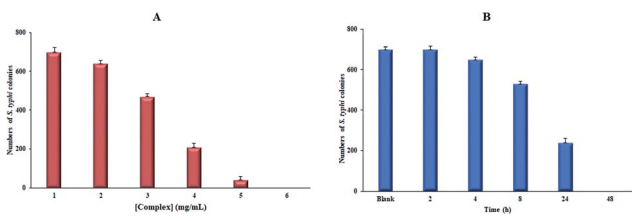

Fig. 13 The increase amount of bacterial colonies (A) as an effect of the Sm complex concentration with 700 CFU of *S. typhi*. (B) as an effect of the inoculation time of the Sm-complex with 700 CFU of *S. typhi*.

4. Conclusion

In this study, the strength and mechanism of the interaction of the Sm complex with DNA and BSA were comprehensively examined by different methods, including electronic spectroscopy, fluorescence spectra, and docking examinations. DNA binding studies suggested that the Sm-complex interacts with the minor groove, which was further affirmed by theoretical investigations. The K_b values showed the high tendency of FS-DNA to bind the Sm complex. The study of the interaction of BSA to the Sm-complex proved that the binding process is driven by enthalpy and is spontaneous. Also, the primary binding forces are hydrogen bonding and van der Waals interactions. According to the site marker competitive study and docking results, the Sm complex bound to BSA in subdomain IB (site III). Additionally, this complex illustrates significant antifungal and antibacterial properties. Also, the drug carrier forms of the Sm complex (SNEP and LNEP) were prepared. All of these compounds exhibited significant antitumor properties against the cell lines, A-549 and MCF-7. The anticancer activity of LNEP and SNEP was higher than that of the Sm complex because of their higher cellular diffusion. The findings of this paper suggest the Sm complex as a suitable candidate for potential applications as an antitumor and antimicrobial agent.

Conflicts of interest

The authors declare that they have no known competing financial interests or personal relationships that could have

appeared to influence the work reported in this paper. Also, there are no conflicts of interest.

Acknowledgements

This paper has been financially supported by the research deputy of the University of Shahrekord (the grant number = 141/2753).

References

1 Z.-F. Chen, M.-X. Tan, Y.-C. Liu, Y. Peng, H.-H. Wang, H.-G. Liu and H. Liang, Synthesis, characterization and preliminary cytotoxicity evaluation of five lanthanide(III)–plumbagin complexes, *J. Inorg. Biochem.*, 2011, **105**(3), 426–434.

2 I. Kostova and T. Stefanova, Synthesis, characterization and cytotoxic/cytostatic activity of La(III) and Dy(III) complexes, *J. Trace Elem. Med. Biol.*, 2010, **24**(1), 7–13.

3 K. H. Thompson and C. Orvig, Editorial: Lanthanide compounds for therapeutic and diagnostic applications, *Chem. Soc. Rev.*, 2006, **35**(6), 499.

4 S. P. Fricker, The therapeutic application of lanthanides, *Chem. Soc. Rev.*, 2006, **35**(6), 524–533.

5 T. Premkumar and S. Govindarajan, Antimicrobial study on trivalent lighter rare-earth complexes of 2-pyrazinecarboxylate with hydrazinium cation, *World J. Microbiol. Biotechnol.*, 2006, **22**(10), 1105–1108.

6 A. J. Amoroso and S. J. A. Pope, Using lanthanide ions in molecular bioimaging, *Chem. Soc. Rev.*, 2015, **44**(14), 4723–4742, DOI: 10.1039/C4CS00293H.

7 A. Cârâc, R. Boscencu, R. M. Dinică, J. F. Guerreiro, F. Silva, F. Marques, M. P. C. Campello, C. Moise, O. Brîncoveanu and M. Enăchescu, Synthesis, characterization and antitumor activity of two new dipyridinium ylide based lanthanide(III) complexes, *Inorg. Chim. Acta*, 2018, **480**, 83–90.

8 K. Raja, A. Suseelamma and K. H. Reddy, Synthesis, spectral properties and DNA binding and nuclease activity of lanthanide(III) complexes of 2-benzoylpyridine benzhydrazone: X-ray crystal structure, Hirshfeld studies and nitrate-π interactions of cerium(III) complex, *J. Chem. Sci.*, 2016, **128**(1), 23–35.

9 D. Yinhua, M. M. Foroughi, Z. Aramesh-Boroujeni, S. Jahani, M. Peydayesh, F. Borhani, M. Khatami, M. Rohani, M. Dusek and V. Eigner, The synthesis, characterization, DNA/BSA/HSA interactions, molecular modeling, antibacterial properties, and *in vitro* cytotoxic activities of novel parent and niosome nano-encapsulated Ho(III) complexes, *RSC Adv.*, 2020, **10**(39), 22891–22908, DOI: 10.1039/D0RA03436C.

10 X. Hu, Z. Tong, Y. Wang, D. Liao, Y. Yin and F. Wen, Investigation of the interaction between protein and europium doped polymer, *J. Macromol. Sci., Part A: Pure Appl.Chem.*, 2019, **56**(1), 42–51.

11 Z. Aramesh-Boroujeni, A.-K. Bordbar, M. Khorasani-Motlagh, N. Fani, E. Sattarinezhad and M. Noroozifar, Computational and experimental study on the interaction of three novel rare earth complexes containing 2,9-dimethyl-1,10-phenanthroline with human serum albumin, *J. Iran. Chem. Soc.*, 2018, **15**(7), 1581–1591, DOI: 10.1007/s13738-018-1356-5.

12 Z. Aramesh-Boroujeni, A.-K. Bordbar, M. Khorasani-Motlagh, E. Sattarinezhad, N. Fani and M. Noroozifar, Synthesis, characterization, and binding assessment with human serum albumin of three bipyridine lanthanide(III) complexes, *J. Biomol. Struct. Dyn.*, 2019, **37**(6), 1438–1450, DOI: 10.1080/07391102.2018.1464959.

13 Z. Aramesh-Boroujeni, S. Jahani, M. Khorasani-Motlagh, K. Kerman, N. Aramesh, S. Asadpour and M. Noroozifar, Experimental and theoretical investigations of Dy(III) complex with 2,2′-bipyridine ligand: DNA and BSA interactions and antimicrobial activity study, *J. Biomol. Struct. Dyn.*, 2019, 1–18, DOI: 10.1080/07391102.2019.1689170.

14 Z. Aramesh-Boroujeni, S. Jahani, M. Khorasani-Motlagh, K. Kerman and M. Noroozifar, Evaluation of DNA, BSA binding, DNA cleavage and antimicrobial activity of ytterbium(III) complex containing 2,2'-bipyridine ligand, *J. Biomol. Struct. Dyn.*, 2020, **38**(6), 1711–1725, DOI: 10.1080/07391102.2019.1617788.

15 Z. Aramesh-Boroujeni, S. Jahani, M. Khorasani-Motlagh, K. Kerman and M. Noroozifar, Evaluation of parent and nano-encapsulated terbium(III) complex toward its photoluminescence properties, FS-DNA, BSA binding affinity, and biological applications, *J. Trace Elem. Med. Biol.*, 2020, **61**, 126564, DOI: 10.1016/j.jtemb.2020.126564.

16 Z. Aramesh-Boroujeni, N. Aramesh, S. Jahani, M. Khorasani-Motlagh, K. Kerman and M. Noroozifar, Experimental and computational interaction studies of terbium(III) and lanthanide(III) complexes containing 2,2′-bipyridine with bovine serum albumin and their *in vitro* anticancer and antimicrobial activities, *J. Biomol. Struct. Dyn.*, 2020, 1–12, DOI: 10.1080/07391102.2020.1792988.

17 Z. Aramesh-Boroujeni, S. Jahani, M. Khorasani-Motlagh, K. Kerman and M. Noroozifar, Parent and nano-encapsulated ytterbium(III) complex toward binding with biological macromolecules, *in vitro* cytotoxicity, cleavage and antimicrobial activity studies, *RSC Adv.*, 2020, **10**(39), 23002–23015, DOI: 10.1039/D0RA03895D.

18 H. A. Hussain, A. A. Ansari and K. Iftikhar, Optical absorption and NMR spectroscopic studies on paramagnetic trivalent lanthanide complexes with 2,2′-bipyridine.: the solvent effect on 4f–4f hypersensitive transitions, *Spectrochim. Acta, Part A*, 2004, **60**(4), 873–884.

19 H.-J. Yu, S.-M. Huang, L.-Y. Li, H.-N. Jia, H. Chao, Z.-W. Mao, J.-Z. Liu and L.-N. Ji, Synthesis, DNA-binding and photocleavage studies of ruthenium complexes $[Ru(bpy)_2(mitatp)]^{2+}$ and $[Ru(bpy)_2(nitatp)]^{2+}$, *J. Inorg. Biochem.*, 2009, **103**(6), 881–890, DOI: 10.1016/j.jinorgbio.2009.03.005.

20 M. Anjomshoa, S. J. Fatemi, M. Torkzadeh-Mahani and H. Hadadzadeh, DNA- and BSA-binding studies and anticancer activity against human breast cancer cells (MCF-7) of the zinc(II) complex coordinated by 5,6-

diphenyl-3-(2-pyridyl)-1,2,4-triazine, *Spectrochim. Acta, Part A*, 2014, **127**, 511–520, DOI: 10.1016/j.saa.2014.02.048.

21 E. Moradinia, M. Mansournia, Z. Aramesh-Boroujeni and A. K. Bordbar, New transition metal complexes of 9,10-phenanthrenequinone *p*-toluyl hydrazone Schiff base: synthesis, spectroscopy, DNA and HSA interactions, antimicrobial, DFT and docking studies, *Appl. Organomet. Chem.*, 2019, **33**(5), e4893, DOI: 10.1002/aoc.4893.

22 F. Neese, The ORCA program system, *Wiley Interdiscip. Rev.: Comput. Mol. Sci.*, 2012, **2**(1), 73–78.

23 G. M. Morris, D. S. Goodsell, R. S. Halliday, R. Huey, W. E. Hart, R. K. Belew and A. J. Olson, Automated docking using a Lamarckian genetic algorithm and an empirical binding free energy function, *J. Comput. Chem.*, 1998, **19**(14), 1639–1662.

24 S. Dianat, A. Bordbar, S. Tangestaninejad, B. Yadollahi, S. Zarkesh-Esfahani and P. Habibi, *In vitro* antitumor activity of parent and nano-encapsulated mono cobalt-substituted Keggin polyoxotungstate and its ctDNA binding properties, *Chem.-Biol. Interact.*, 2014, **215**, 25–32.

25 M. Mohamadi, A. Hassankhani, S. Y. Ebrahimipour and M. Torkzadeh-Mahani, *In vitro* and *in silico* studies of the interaction of three tetrazoloquinazoline derivatives with DNA and BSA and their cytotoxicity activities against MCF-7, HT-29 and DPSC cell lines, *Int. J. Biol. Macromol.*, 2017, **94**, 85–95, DOI: 10.1016/j.ijbiomac.2016.09.113.

26 A. Abbasi Kajani, A.-K. Bordbar, M. A. Mehrgardi, S. H. Zarkesh-Esfahani, H. Motaghi, M. Kardi, A. R. Khosropour, J. Ozdemir, M. Benamara and M. H. Beyzavi, Green and Facile Synthesis of Highly Photoluminescent Multicolor Carbon Nanocrystals for Cancer Therapy and Imaging, *ACS Appl. Bio Mater.*, 2018, **1**(5), 1458–1467.

27 E. Köksal, H. Tohma, Ö. Kılıç, Y. Alan, A. Aras, I. Gülçin and E. Bursal, Assessment of antimicrobial and antioxidant activities of *Nepeta trachonitica*: analysis of its phenolic compounds using HPLC-MS/MS, *Sci. Pharm.*, 2017, **85**(2), 24.

28 U. M. Kocyigit, Y. Budak, M. B. Gürdere, N. Dürü, P. Taslimi, İ. Gülçin and M. Ceylan, Synthesis and investigation of anticancer, antibacterial activities and carbonic anhydrase, acetylcholinesterase inhibition profiles of novel (3aR, 4S, 7R, 7aS)-2-[4-[1-acetyl-5-(aryl/heteroaryl)-4,5-dihydro-1*H*-pyrazol-3-yl]phenyl]-3a, 4, 7, 7a-tetrahydro-1H-4,7-methanoisoindole-1,3(2*H*)-diones, *Monatsh. Chem.*, 2019, **150**(4), 721–731.

29 S. Jahani, M. Khorasani-Motlagh and M. Noroozifar, DNA interaction of europium(III) complex containing 2,2′-bipyridine and its antimicrobial activity, *J. Biomol. Struct. Dyn.*, 2016, **34**(3), 612–624.

30 W.-Z. Shen, G. Trötscher-Kaus and B. Lippert, 1H NMR spectroscopic identification of binding modes of 2,2′-bipyridine ligands in complexes of square-planar d 8 metal ions, *Dalton Trans.*, 2009, **39**, 8203–8214.

31 A. Haque, I. Khan, S. I. Hassan and M. S. Khan, Interaction studies of cholinium-based ionic liquids with calf thymus DNA: spectrophotometric and computational methods, *J. Mol. Liq.*, 2017, **237**, 201–207.

32 D. He, L. Wang, L. Wang, X. Li and Y. Xu, Spectroscopic studies on the interactions between novel bisnaphthalimide derivatives and calf thymus DNA, *J. Photochem. Photobiol., B*, 2017, **166**, 333–340, DOI: 10.1016/j.jphotobiol.2016.12.003.

33 U. Chaveerach, A. Meenongwa, Y. Trongpanich, C. Soikum and P. Chaveerach, DNA binding and cleavage behaviors of copper(II) complexes with amidino-O-methylurea and N-methylphenyl-amidino-O-methylurea, and their antibacterial activities, *Polyhedron*, 2010, **29**(2), 731–738, DOI: 10.1016/j.poly.2009.10.031.

34 N. Shahabadi and M. Falsafi, Experimental and molecular docking studies on DNA binding interaction of adefovir dipivoxil: Advances toward treatment of hepatitis B virus infections, *Spectrochim. Acta, Part A*, 2014, **125**, 154–159.

35 F. Cui, G. Hui, X. Jiang and G. Zhang, Interaction of 3′-azido-3′-deamino daunorubicin with DNA: multispectroscopic and molecular modeling, *Int. J. Biol. Macromol.*, 2012, **50**(4), 1121–1126.

36 B.-L. Wang, D.-Q. Pan, K.-L. Zhou, Y.-Y. Lou and J.-H. Shi, Multi-spectroscopic approaches and molecular simulation research of the intermolecular interaction between the angiotensin-converting enzyme inhibitor (ACE inhibitor) benazepril and bovine serum albumin (BSA), *Spectrochim. Acta, Part A*, 2019, **212**, 15–24.

37 F. Jalali and P. S. Dorraji, Interaction of anthelmintic drug (thiabendazole) with DNA: spectroscopic and molecular modeling studies, *Arabian J. Chem.*, 2017, **10**, S3947–S3954, DOI: 10.1016/j.arabjc.2014.06.001.

38 T. Sarwar, H. M. Ishqi, S. U. Rehman, M. A. Husain, Y. Rahman and M. Tabish, Caffeic acid binds to the minor groove of calf thymus DNA: a multi-spectroscopic, thermodynamics and molecular modelling study, *Int. J. Biol. Macromol.*, 2017, **98**, 319–328, DOI: 10.1016/j.ijbiomac.2017.02.014.

39 X.-B. Fu, Z.-H. Lin, H.-F. Liu and X.-Y. Le, A new ternary copper(II) complex derived from 2-(2′-pyridyl) benzimidazole and glycylglycine: synthesis, characterization, DNA binding and cleavage, antioxidation and HSA interaction, *Spectrochim. Acta, Part A*, 2014, **122**, 22–33.

40 S. Yadav, I. Yousuf, M. Usman, M. Ahmad, F. Arjmand and S. Tabassum, Synthesis and spectroscopic characterization of diorganotin (IV) complexes of *N*′-(4-hydroxypent-3-en-2-ylidene) isonicotinohydrazide: chemotherapeutic potential validation by *in vitro* interaction studies with DNA/HSA, DFT, molecular docking and cytotoxic activity, *RSC Adv.*, 2015, **5**(63), 50673–50690.

41 F. A. Qais, K. Abdullah, M. M. Alam, I. Naseem and I. Ahmad, Interaction of capsaicin with calf thymus DNA: a multi-spectroscopic and molecular modelling study, *Int. J. Biol. Macromol.*, 2017, **97**, 392–402.

42 G.-F. Shen, T.-T. Liu, Q. Wang, M. Jiang and J.-H. Shi, Spectroscopic and molecular docking studies of binding interaction of gefitinib, lapatinib and sunitinib with bovine serum albumin (BSA), *J. Photochem. Photobiol., B*, 2015, **153**, 380–390.

43 Q. Gan, X. Fu, W. Chen, Y. Xiong, Y. Fu, S. Chen and X. Le, Synthesis, DNA/HSA interaction spectroscopic studies and *in vitro* cytotoxicity of a new mixed ligand Cu(II) complex, *J. Fluoresc.*, 2016, **26**(3), 905–918.

44 A. T. Buddanavar and S. T. Nandibewoor, Multi-spectroscopic characterization of bovine serum albumin upon interaction with atomoxetine, *Arabian J. Chem.*, 2017, **7**(3), 148–155.

45 P. Bolel, N. Mahapatra and M. Halder, Optical spectroscopic exploration of binding of cochineal red A with two homologous serum albumins, *J. Agric. Food Chem.*, 2012, **60**(14), 3727–3734.